The Regulation of Angular Momentum During Human Walking

by

Jianwen Wendy Gu

Submitted to the Department of Physics
in partial fulfillment of the requirements for the degree of
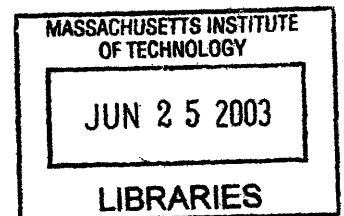
Bachelor of Science

at the

MASSACHUSETTS INSTITUTE OF TECHNOLOGY

June 2003

© Jianwen Wendy Gu, MMIII. All rights reserved.

The author hereby grants to MIT permission to reproduce and
distribute publicly paper and electronic copies of this thesis document
in whole or in part.

Author ....
Department of Physics
May 9, 2003

Certified by...
Hugh M. Herr
Assistant Professor, Department of Health Sciences and Technology
Thesis Supervisor

Accepted by ....
Professor David E. Pritchard
Senior Thesis Coordinator, Department of Physics

The Regulation of Angular Momentum During Human Walking

by

Jianwen Wendy Gu

Abstract

The conservation of angular momentum provides an elegant model for human walking and might be used to generate stable robotic locomotion if employed by a control algorithm. To examine the extent to which the body regulates angular momentum, a force model was developed to predict horizontal ground reaction forces assuming perfect angular momentum conservation. These model forces closely matched experimental forces, suggesting that the body does indeed regulate angular momentum. To determine how various links of the body contribute to total angular momentum, link angular momenta were calculated. Angular momenta in the medial-lateral and vertical directions showed evident cancellation of link angular momenta whereas angular momentum in the anterior-posterior direction did not. Link by link, angular momentum in the medial-lateral direction was much larger than angular momenta in the anterior-posterior and vertical directions, which makes it more likely to cause stability problems. Hence, angular momentum in the medial-lateral direction is the key angular momentum to regulate.

Thesis Supervisor: Hugh M. Herr
Title: Assistant Professor, Department of Health Sciences and Technology

Acknowledgments

Contents

List of Figures

List of Tables

Chapter 1

Introduction

1.1   Background

The mechanics of walking and running are complicated, as exemplified by the difficulties involved in building robots that can emulate human walking. The first step in dissecting any complex system is to search for an underlying principle that governs the functioning of that system. In the case of rigid moving bodies, angular momentum about the center of mass (CM) is a fundamental physical quantity related to the torque applied to the CM. Specifically, angular momentum is conserved in the CM frame if the sum of external torques about the CM is zero. During the aerial phase of human locomotion (for example, when both feet are off the ground during running), the only force acting on the body is gravity, which acts through the CM, resulting in zero torque. Thus, angular momentum is conserved. However, the interaction of the feet with the ground during walking introduces external torques about the CM, so there is no *a priori* reason for angular momentum to be conserved.

1.2   Motivation

Angular momentum during human locomotion has been studied, but it has not been investigated thoroughly for normal human walking. Much research done on angular momentum thus far is related to sports. Dapena and McDonald analyzed angular

momentum during the hammer throw in 1989 [2]. In 1993 Dapena studied angular momentum in the discus throw [1], and LeBlanc and Dapena investigated angular momentum during the javelin throw in 1996 [9]. Angular momentum in these sports has little relevance to angular momentum during normal human locomotion.

Hinrichs and colleagues studied angular momentum of the arms during running in 1983. They found that arm angular momentum reduced leg angular momentum in the vertical direction during running and that angular momenta of the arms in the other two directions tended to cancel each other. [5] Hinrichs corroborated these results in a similar study in 1987 [3]. In 1992 he did case studies of asymmetric arm action during running, finding that runners with an asymmetric arm angular momentum profile in the vertical direction still had a symmetric total arm angular momentum profile. Based on these results, he suggested that one arm has the potential to compensate for the other in generating angular momentum in the vertical direction. [4] However, Hinrichs and collaborators did not do a detailed analysis of lower body angular momentum, and they considered only running, which is a less fundamental form of locomotion than walking.

In 1998 Xu and Wang quantified angular momentum changes during walking [13]. However, they studied only the lower body, and we believe that the entire body must be considered to shed insight on how the body regulates angular momentum.

Riley and colleagues in 1997 studied angular momentum of thirteen elderly subjects who suffered sit-to-stand failures and thirteen who did not. They found that the angular momentum profile of those who lost their balance during sit-to-stand differed from that of the control subjects. [10] Their work suggests that regulation of angular momentum is integral to balancing.

In 2000 Simoneau and Krebs studied whole-body angular momentum during walking in five elderly subjects, three considered "non-fallers" and two considered "frequent fallers." They found that angular momentum characteristics for the two groups were similar whereas the ankle and knee torques of the "frequent fallers" were smaller than those of the "non-fallers." They suggested that the inability to control angular momentum with the appropriate torques leads to falling. [12] One weakness of their

14

study is the limited number of subjects in each category. In addition, they looked only at whole-body angular momentum without investigating individual link angular momentum.

Angular momentum has been used to control bipedal robotic walking. Sano and Furusho produced more natural walking by monitoring and controlling the angular momentum of their bipedal robot in 1990. They used ankle torque of the stance leg to produce a desired angular momentum function that was based on changes in angular momentum undergone by an inverted pendulum in gravity. [11] However, they considered only angular momentum for sagittal plane rotations and used a somewhat arbitrary function for the desired angular momentum. A better understanding of how angular momentum is regulated by the human body may enable robotic engineers to better design control algorithms for robotic walking.

Kajita and colleagues in 2001 used control of angular momentum to balance their humanoid robot while it stood on one leg. They used ankle torque to minimize angular momentum associated with sagittal and coronal plane rotations. [8] However, they did not consider balance during walking. Again, knowledge of how the human body regulates angular momentum might aid robotic engineers in producing biologically real behavior in balancing or walking robots.

The aim of this work is to expose an underlying principle governing human locomotion. We hypothesized that total body angular momentum in the CM frame is highly regulated, and we tested this hypothesis by collecting and analyzing kinematic and kinetic data on five subjects walking at self-selected speeds. One specific improvement to previous work is that total body angular momentum during walking was considered instead of only upper or lower body angular momentum. Also, angular momentum in all three directions was examined instead of only angular momentum in one or two directions. Furthermore, link angular momenta were calculated to investigate the partition of angular momentum throughout the human body (in other words, how various links combine to give total angular momentum). Besides providing an elegant model for human locomotion, the conservation of angular momentum, if used as a control objective, might produce stable robotic locomotion with enhanced

15

biological realism.

Chapter 2

Force Analysis

2.1 Force Model

A model was developed to predict the ground reaction force (GRF), which is the force that the ground exerts on the body during locomotion, if angular momentum about the body CM were conserved. The forces between the feet and ground can be summed to yield a single GRF vector $\vec{F}$ that acts on a point on the ground called the center of pressure (CP). The torque $\vec{T}$ about the body CM due to the GRF is therefore $\vec{r} \times \vec{F}$, where $\vec{r}$ is the vector from the body CM to the CP. Angular momentum $\vec{L}$ of a point mass, say the CM of a foot, about the body CM is defined as $\vec{r} \times \vec{p}$, where $\vec{p}$ is momentum of the point mass. Force is change of momentum over time, which leads to the following equation relating torque and change of angular momentum over time:

$$\vec{T} = \vec{r} \times \vec{F} = \vec{r} \times \frac{d\vec{p}}{dt} = \frac{d\vec{L}}{dt}. \tag{2.1}$$

If angular momentum is conserved, $\frac{d\vec{L}}{dt}$ in Equation 2.1 goes to zero and torque must be zero as well. This provides a constraint on the GRF:

$$\vec{T} = \vec{0} = \vec{r} \times \vec{F} \tag{2.2}$$

or written in component form,

$$\mathcal{T}_x = 0 = r_y F_z - r_z F_y \tag{2.3}$$

$$\mathcal{T}_y = 0 = r_z F_x - r_x F_z \tag{2.4}$$

$$\mathcal{T}_z = 0 = r_x F_y - r_y F_x. \tag{2.5}$$

Solving Equations 2.3 and 2.4 for F_y and F_x, respectively, gives

$$F_x = \frac{F_z}{r_z} r_x \tag{2.6}$$

$$F_y = \frac{F_z}{r_z} r_y. \tag{2.7}$$

Equations 2.6 and 2.7 predict the x and y components of the GRF from the z component of the GRF and components of the vector from the body CM to the CP. These equations were derived assuming perfect angular momentum conservation, which allows the quantification of the level of angular momentum regulation. This can be accomplished by measuring GRF during walking and comparing the results to model predictions. Specifically, Fz, r_z, r_x, and r_y in Equations 2.6 and 2.7 were experimentally determined to predict F_x and F_y using those equations. The predicted F_x and F_y were compared to experimental measurements of F_x and F_y. A higher correlation between model predictions and experimental measurements indicates a greater degree of angular momentum regulation.

2.2 Human Model

A model of the human body was created using *Creature Library* (*CL*) and *SD/FAST*. *CL* is software developed in the Leg Laboratory of the MIT Artificial Intelligence Laboratory that provides an accessible user interface for *SD/FAST*, commercial software that simulates systems composed of rigid bodies. The size and shape of a system (in this case, the human body) is specified using *CL*, which then works with SD/FAST to generate physical parameters such as mass and moment of inertia of each com-

18

ponent of that system (the head, body, and limbs). The human model is shown in Figure 2-1. The model of the human body consisted of thirteen links (pair of feet, pair of shanks, pair of thighs, pair of hands, pair of forearms, pair of upper arms, and trunk and head) with twelve joints (pair of ankles, pair of knees, pair of hips, pair of wrists, pair of elbows, and pair of shoulders). The feet and hands were modeled as rectangular boxes; the shanks, thighs, forearms, and upper arms as truncated cones; and the trunk and head as a cylinder with an elliptical cross-section with a sphere on top.
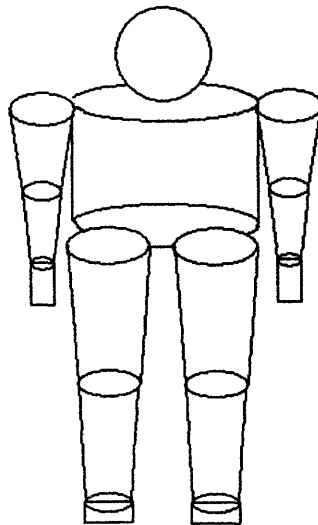
Figure 2-1: *Human model created in Creature Library.* The model consists of thirteen links (pair of feet, pair of shanks, pair of thighs, pair of hands, pair of forearms, pair of upper arms, and trunk and head) with twelve joints (pair of ankles, pair of knees, pair of hips, pair of wrists, pair of elbows, and pair of shoulders). The feet and hands are modeled as rectangular boxes; the shanks, thighs, forearms, and upper arms as truncated cones; and the trunk and head as a cylinder with an elliptical cross-section with a sphere on top.

Subject	Sex	Age	Weight (kg)	Walking Speed (m/s)
1	female	21	50.1	1.29 ± 0.02
2	female	21	49.9	1.05 ± 0.01
3	female	21	62.7	1.35 ± 0.05
4	male	24	82.6	1.25 ± 0.03
5	male	31	76.8	1.32 ± 0.04

Table 2.1: *Physical characteristics of experimental subjects.* Five subjects participated in the walking and hip rotation experiments. There were three female and two male subjects, who ranged in age from 21 to 31 years, in weight from 49.9 to 82.6 kg, and in walking speed from 1.05 to 1.35 m/s.

2.3 Data Collection

Data were gathered in the Gait Laboratory of Spaulding Rehabilitation Hospital in a study approved by the MIT Committee on the Use of Humans as Experimental Subjects. Five subjects participated in the experiments; their physical characteristics are shown in Table 2.1. Physical measurements of the subject's links were taken to accurately model the subject. Markers were placed on various parts of the subject's body: sixteen lower body markers, five trunk markers, eight upper limb markers, and four head markers. An infrared Vicon Motion Capture System recorded the marker positions as the subject moved about the testing platform. Two force plates in the center of the platform recorded GRF and CP measurements when the subject stepped on them. The subject walked at a self-selected speed for six or seven trials, each trial consisting of one traversal of the testing platform. In a different experiment, the subject started from standing and rotated his or her hips (similar to how one twirls a hula hoop) at an increasing speed for ten seconds. Figure 2-2 shows the coordinate system used in analyzing the data. x is defined as the forward direction, y points toward the left from the subject's perspective, and z is in the vertical direction. Figure 2-3 shows an overview of the analysis done on the data.
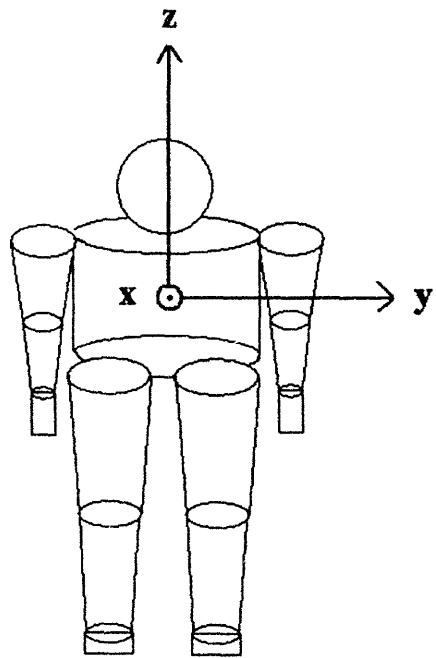
Figure 2-2: *Coordinate system of walking experiment.* x is defined as the forward direction, y points toward the left from the subject's perspective, and z is in the vertical direction.
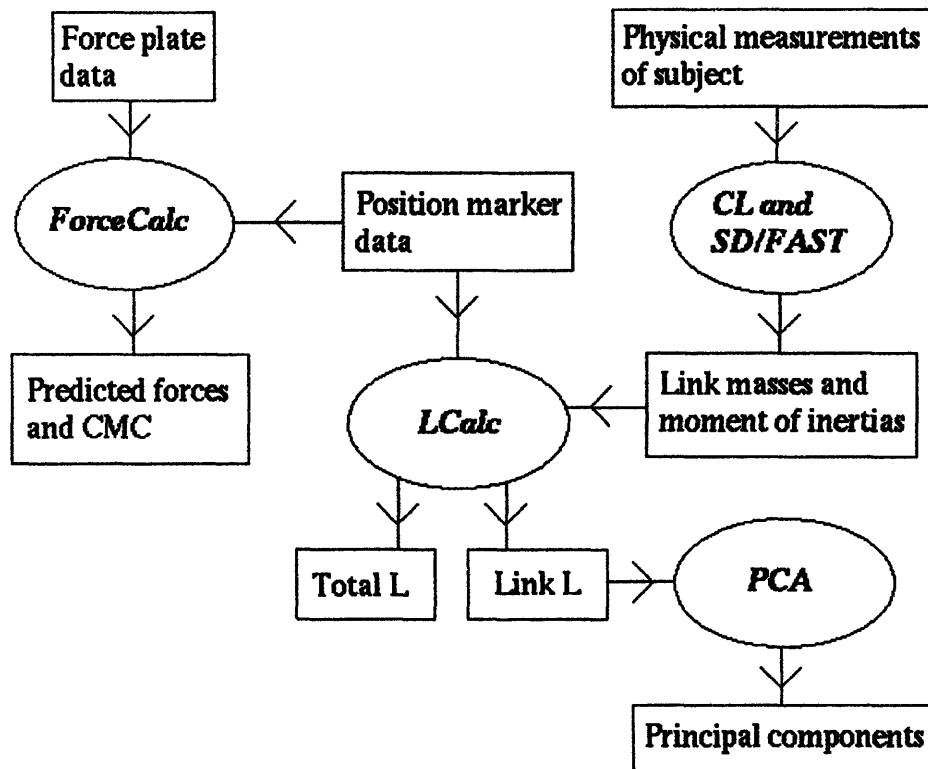
Figure 2-3: *Overview of data analysis.* Software programs are in ovals, and data are in boxes. Arrows indicate the flow of data.

2.4 Calculation of Predicted Forces

A program *ForceCalc* was developed for calculating the forces predicted by Equations 2.6 and 2.7 from the data gathered in the Gait Laboratory using Matlab. *Force-Calc* determined the body CM position from the marker position data and the link masses given by *Creature Library* and *SD/FAST*. It subtracted the body CM position from the CP position to obtain $\vec{r}$, which was used along with F_z provided by the force plates to calculate F_x and F_y using Equations 2.6 and 2.7. These forces were compared to the experimental F_x and F_y measured by the force plates in the Gait Laboratory. For each subject, data from all trials were combined to give the coefficient of multiple correlation (CMC), a statistical measure of how well the model and

22

experimental forces correlated. A *CMC* of 1 means 100% similarity (for example, two sine waves that are in phase) and a *CMC* of 0 implies no correlation between waveforms (for example, two sine waves that are 180° out of phase). The *CMC* was developed by Kadaba and colleagues to quantify the repeatability of kinematic data in normal adult gait. The *CMC* is given by

$$CMC = \sqrt{1 - \frac{\sum_{i=1}^{M}\sum_{j=1}^{N}\sum_{t=1}^{T}(Y_{ijt} - \bar{Y}_{it})^2/MT(N-1)}{\sum_{i=1}^{M}\sum_{j=1}^{N}\sum_{t=1}^{T}(Y_{ijt} - \bar{Y}_i)^2/M(NT-1)}} \qquad (2.8)$$

where Y_{ijt} is the value of the kinematic variable at the tth time point of the jth trial on the ith test day. M is the total number of test days, N is the total number of trials on the ith test day, and T is the total number of time points in the jth trial. $\bar{Y}_{it}$ is the average of the variable at time point t on the ith test day and is given by

$$\bar{Y}_{it} = \frac{1}{N}\sum_{j=1}^{N}Y_{ijt}. \qquad (2.9)$$

$\bar{Y}_i$ is the grand mean on the ith day and is given by

$$\bar{Y}_i = \frac{1}{NT}\sum_{j=1}^{N}\sum_{t=1}^{T}Y_{ijt}. \,[7] \qquad (2.10)$$

Equation 2.8 was modified to yield the *CMC* for measuring the similarity between model and experimental forces in our study:

$$CMC = \sqrt{1 - \frac{\sum_{j=1}^{2}\sum_{t=1}^{T}(Y_{jt} - \bar{Y}_t)^2/T}{\sum_{j=1}^{2}\sum_{t=1}^{T}(Y_{jt} - \bar{Y})^2/(2T-1)}} \qquad (2.11)$$

where Y_{1t} is the model force at the tth time point, Y_{2t} is the experimental force at the tth time point, T is the total number of time points, $\bar{Y}_t$ is the mean of the model and experimental forces at the tth time point, and $\bar{Y}$ is the mean of $\bar{Y}_t$ for the trial.

2.5 Results

Figures 2-4 through 2-8 show the model and experimental forces during a sample trial of the walking experiment for each subject. Forces generated by heavier subjects were naturally larger. F_x, the GRF in the direction of walking, was greater than F_y, the GRF perpendicular to the direction of locomotion, for each subject. Model and experimental forces were similar, and the degree of similarity was quantified by the CMC.
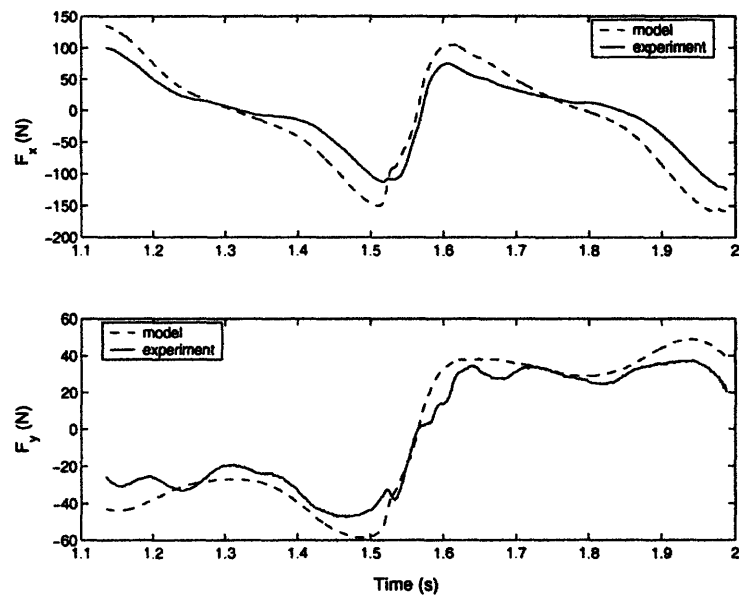

Figure 2-4: *Model and experimental forces during walking vs time (Subject 1)*. The experimental F_x varies from -124 N to 100 N, and the experimental F_y varies from -47 N to 37 N.
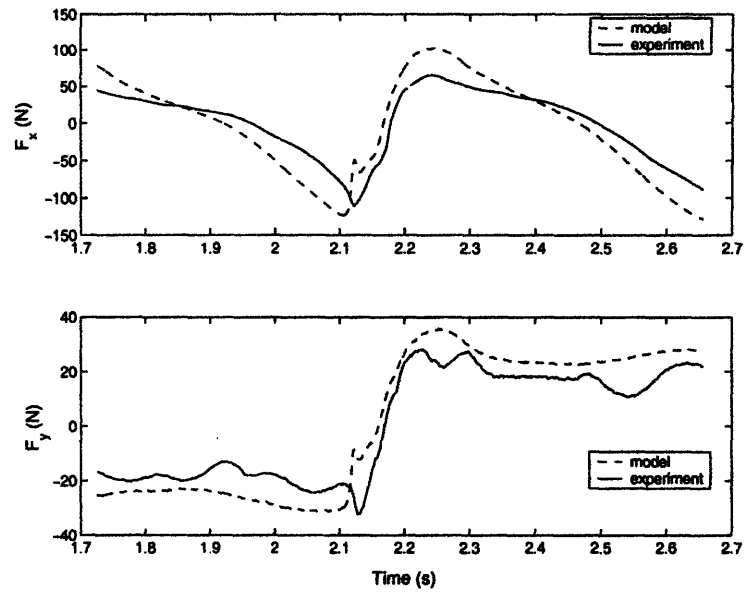
Figure 2-5: *Model and experimental forces during walking vs time (Subject 2).* The experimental F_x varies from -111 N to 66 N, and the experimental F_y varies from -32 N to 28 N.
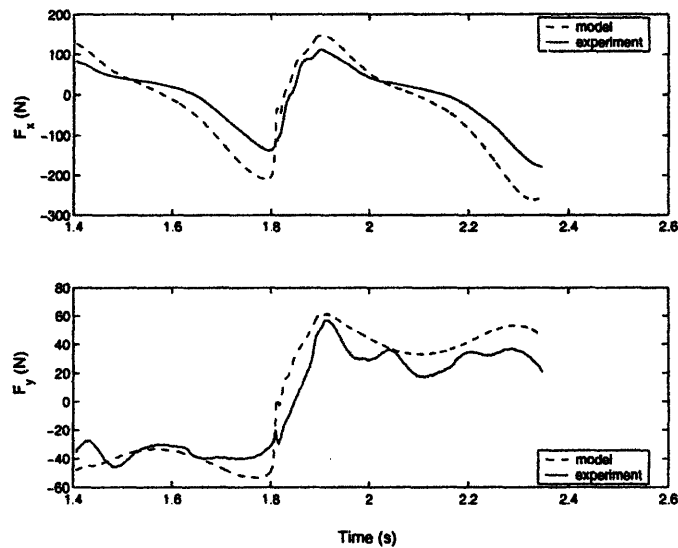

Figure 2-6: *Model and experimental forces during walking vs time (Subject 3).* The experimental F_x varies from -180 N to 112 N, and the experimental F_y varies from -46 N to 57 N.

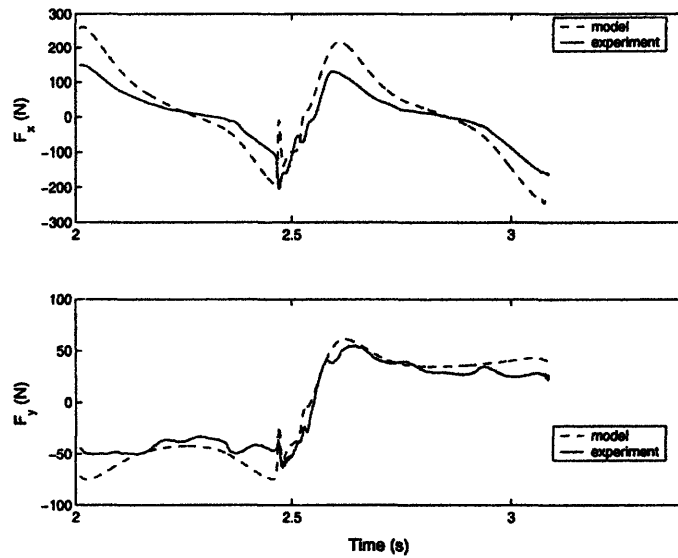25

Figure 2-7: *Model and experimental forces during walking vs time (Subject 4)*. The experimental F_x varies from -204 N to 150 N, and the experimental F_y varies from -64 N to 55 N.
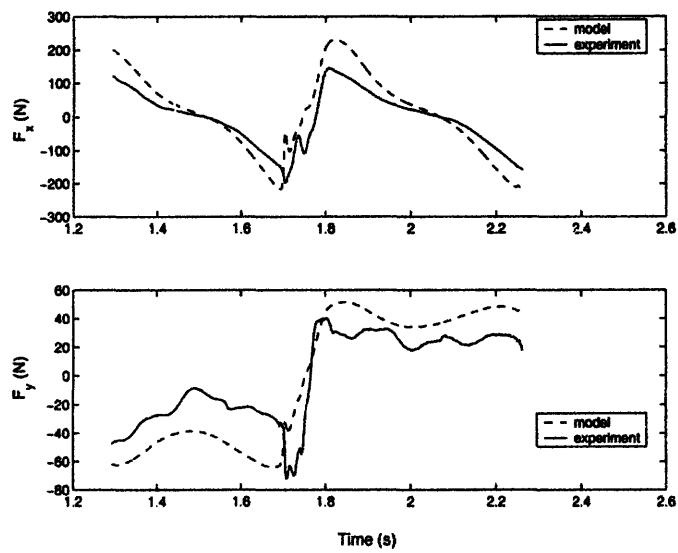

Figure 2-8: *Model and experimental forces during walking vs time (Subject 5)*. The experimental F_x varies from -198 N to 146 N, and the experimental F_y varies from -73 N to 41 N.

26

Subject	CMC for F_x	CMC for F_y
1	0.92	0.98
2	0.89	0.96
3	0.90	0.96
4	0.84	0.95
5	0.87	0.85
Mean	0.88 ± 0.03	0.94 ± 0.05

Table 2.2: *Coefficient of multiple correlation for force analysis.* The mean CMC for F_y (0.94 ± 0.05) is higher than that for F_x (0.88 ± 0.03) and has a larger standard deviation.

Table 2.2 shows the CMC for F_x and F_y of each subject and the mean CMC and standard deviation in CMC across the five subjects. The CMC for each subject was found by combining all the subject's walking trials and using Equation 2.11. Across the five subjects, the mean CMC for F_x was 0.88 ± 0.03, and the mean CMC for F_y was 0.94 ± 0.05. To review, CMC varies between 0 and 1, with 1 corresponding to perfect correlation and 0 corresponding to no correlation.

Model and experimental forces during a trial in the rotation experiment for Subject 3 are shown in Figure 2-9. While the subject was standing or rotating slowly near the beginning of the trial, model and experimental forces were comparable. However, they diverged as rotation of the subject's hips accelerated.
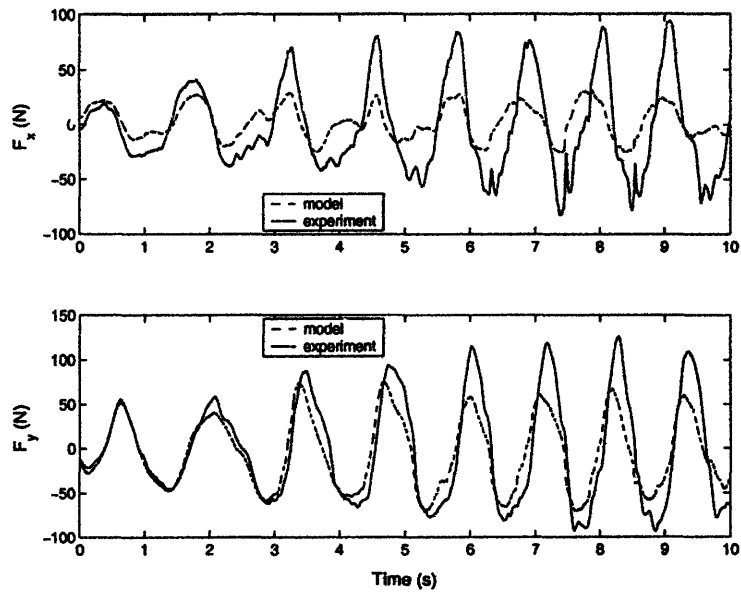
Figure 2-9: *Model and experimental forces during rotation vs time (Subject 3)*. Model and experimental forces are similar when the subject starts the trial with standing, and they become increasingly disparate as the rotation of the subject's hips accelerates. Experimental F_x reaches a maximum of 94 N and experimental F_y reaches a maximum of 126 N at the fastest rotation speed.

2.6 Discussion

Model and experimental ground reaction forces during walking matched closely (Figures 2-4 through 2-8). The degree of correlation was quantified by the CMC (Table 2.2), which measures the similarity between two waveforms. The waveforms were the model GRF predicted in the presence of perfect angular momentum conservation and the experimental GRF measured by the force plates. The mean CMC for F_x across the five subjects was 0.88 ± 0.03 and the mean CMC for F_y was 0.94 ± 0.05. The CMC for F_x was smaller than the CMC for F_y. This makes sense because forces generated in the direction of motion (F_x) were larger and thus more difficult to control such that angular momentum was conserved. However, the CMC for both F_x and F_y was high, supporting the hypothesis that angular momentum is regulated. The disparity between model and experimental forces during the hip rotation experiment (Figure 2-9) indicates that angular momentum conservation is not a necessary condition for stable human motion, which suggests that the body may actively regulate angular momentum during walking.

Chapter 3

Angular Momentum Analysis

3.1 Calculation of Angular Momentum

A program *LCalc* was developed in Matlab for calculating the total angular momentum about the body CM and the individual link angular momenta. First, *LCalc* determined the CM position of each link and found the angular momentum of the link CM about the body CM using position marker and mass data. It then calculated the angular momentum of each link about its own CM using position marker and moment of inertia data. Finally, it added these angular momenta to give the total link angular momentum, which was summed across all links to obtain the total angular momentum about the body CM.

3.2 Principal Components Analysis

Principal components analysis (PCA) was done on the link angular momenta to give the partition of angular momentum throughout the body. PCA is a statistical method that reduces the number of parameters needed to describe a data set. PCA takes a matrix of data in one basis (in this case, the basis of the angular momenta of the body links) and transforms the matrix into a basis that eliminates the covariances of the new variables. The new variables are the principal components (PCs). First, PCA finds the covariance matrix S of the original variables (the link angular momenta of

which there are thirteen):

$$
S = \begin{bmatrix}
s_1^2 & s_{1,2} & \cdots & s_{1,13} \\
s_{2,1} & s_2^2 & \cdots & s_{2,13} \\
\vdots & \vdots & & \vdots \\
s_{13,1} & s_{13,2} & \cdots & s_{13}^2
\end{bmatrix}
\tag{3.1}
$$

where s_i^2 is the variance of the ith variable and $s_{i,j}$ is the covariance between the ith and jth variables. If $s_{i,j}$ is nonzero, a linear relationship exists between the ith and jth variables, which indicates a redundancy in the variables describing the data. PCA seeks to eliminate that redundancy by finding new variables with zero covariances. Since $s_{i,j} = s_{j,i}$, S is a symmetric matrix, and because S is the covariance matrix of real data, it can be assumed to be nonsingular. Linear algebra theory states that any symmetric, nonsingular matrix, such as S, can be reduced to a diagonal matrix L by pre- and post-multiplying it by a particular orthonormal matrix U:

$$
U'SU = L. \tag{3.2}
$$

The diagonal elements of L are the eigenvalues l_i of S, and the columns of U are the eigenvectors u_i of S. By definition, S, u_i, and l_i satisfy

$$
Su_i = l_i u_i, \tag{3.3}
$$

which can be solved easily to find u_i and l_i. Thus, the eigenvectors of S (the PCs) are the new variables written as a linear combination of the original ones, and they form a basis in which the covariance matrix is L. As L is a diagonal matrix, the covariances of the new variables are zero, which is the desired result. PCA orders the PCs such that the diagonal elements of L, the variances of the new variables, decrease along the diagonal. Although there are the same number of PCs as original variables, usually only a subset of these is necessary to account for the variance in the data (in this case, the total angular momentum). [6] Therefore, instead of dealing with thirteen

individual links, we could see how the link angular momenta combined to give the total angular momentum by considering the first few principal components.

3.3 Results

3.3.1 Angular Momentum

The total angular momentum $\vec{L}$ over one gait cycle during walking for each subject is shown in Figures 3-1 through 3-5. A gait cycle starts when the right heel strikes the ground and ends when the right heel hits the ground again in the next step. The trials for each subject were combined to produce a mean angular momentum with error bars given by one standard deviation. Heavier subjects naturally produced greater angular momenta. For each subject, L_y was larger than L_x, and L_z was the smallest of the three.
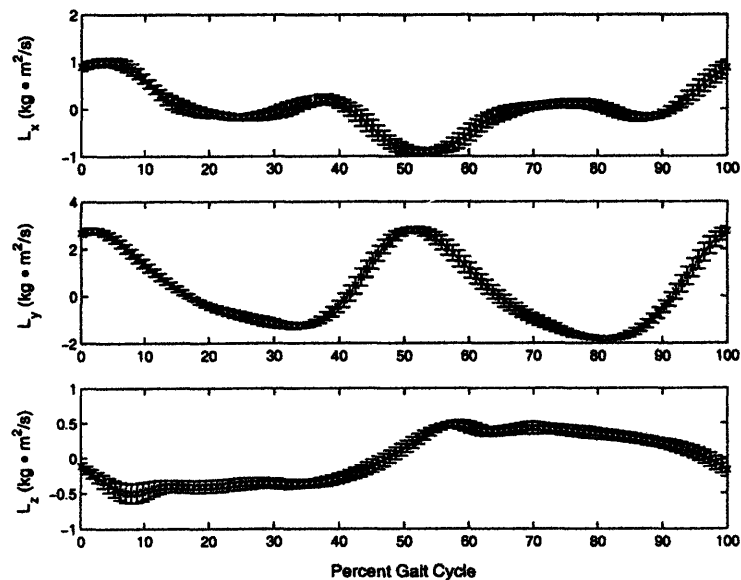

Figure 3-1: *Angular momentum during walking vs percent gait cycle (Subject 1). The seven trials were combined to produce mean angular momenta with error bars given by one standard deviation. L_x varies between -0.9 $kg \cdot m^2/s$ and 1.0 $kg \cdot m^2/s$, L_y between -1.8 $kg \cdot m^2/s$ and 2.8 $kg \cdot m^2/s$, and L_z between -0.5 $kg \cdot m^2/s$ and 0.5 $kg \cdot m^2/s$.*

Figure 3-2: *Angular momentum during walking vs percent gait cycle (Subject 2)*. The six trials were combined to produce mean angular momenta with error bars given by one standard deviation. L_x varies between -0.8 $kg \cdot m^2/s$ and 0.9 $kg \cdot m^2/s$, L_y between -1.6 $kg \cdot m^2/s$ and 3.1 $kg \cdot m^2/s$, and L_z between -0.5 $kg \cdot m^2/s$ and 0.5 $kg \cdot m^2/s$.
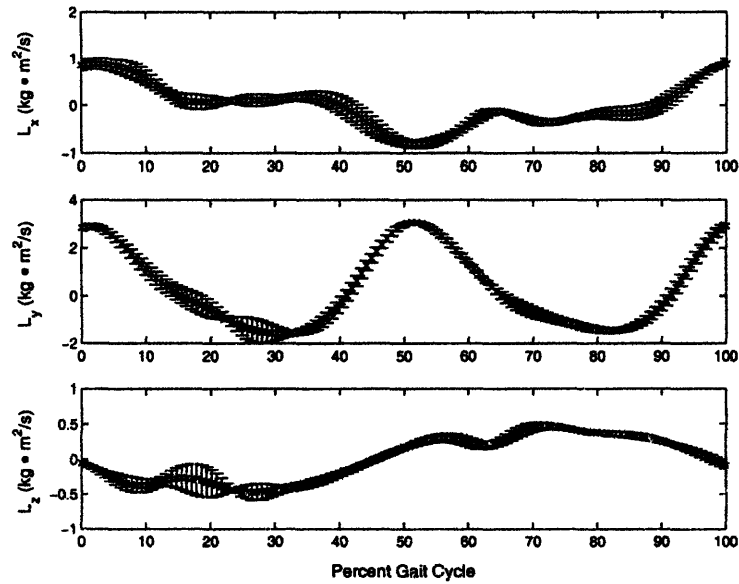

Figure 3-3: *Angular momentum during walking vs percent gait cycle (Subject 3)*. The six trials were combined to produce mean angular momenta with error bars given by one standard deviation. L_x varies between -1.5 $kg \cdot m^2/s$ and 1.6 $kg \cdot m^2/s$, L_y between -2.1 $kg \cdot m^2/s$ and 4.7 $kg \cdot m^2/s$, and L_z between -1.0 $kg \cdot m^2/s$ and 1.1 $kg \cdot m^2/s$.
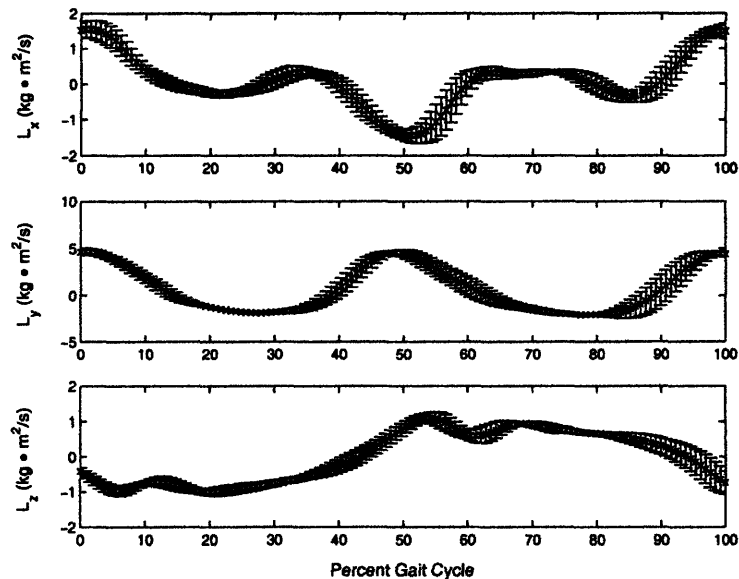
34

Figure 3-4: *Angular momentum during walking vs percent gait cycle (Subject 4)*. The seven trials were combined to produce mean angular momenta with error bars given by one standard deviation. L_x varies between -2.3 $kg \cdot m^2/s$ and 2.5 $kg \cdot m^2/s$, L_y between -3.2 $kg \cdot m^2/s$ and 7.1 $kg \cdot m^2/s$, and L_z between -1.6 $kg \cdot m^2/s$ and 1.5 $kg \cdot m^2/s$.
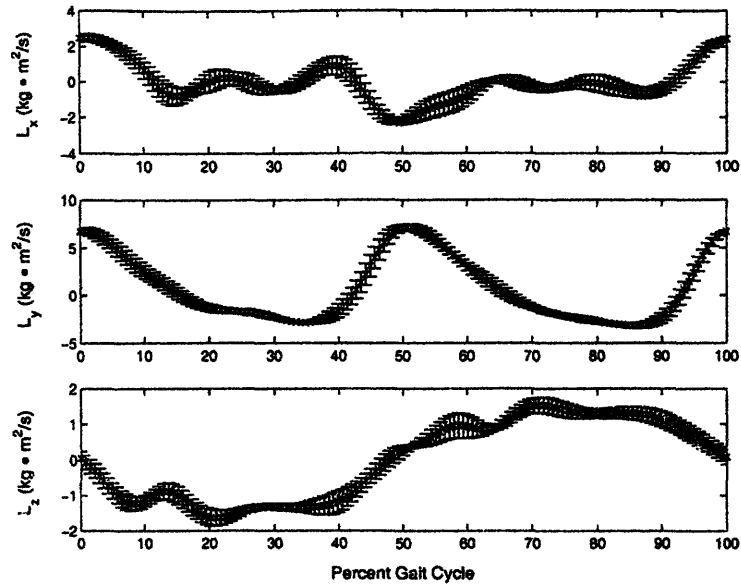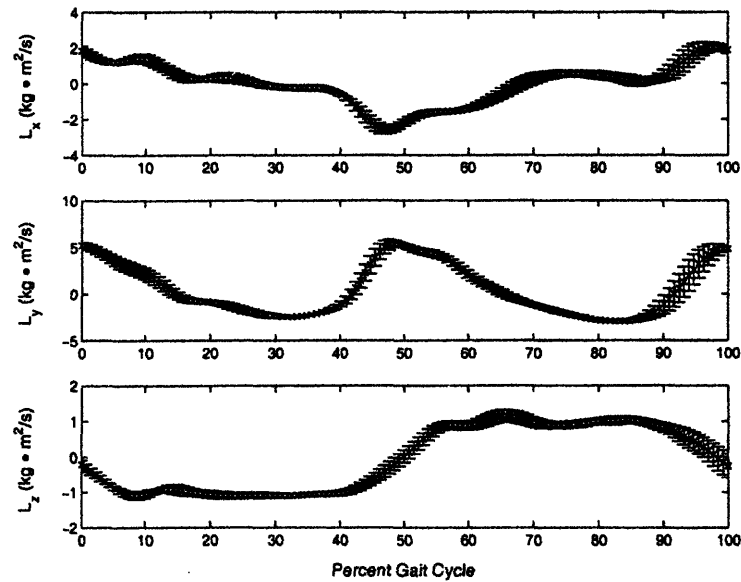

Figure 3-5: *Angular momentum during walking vs percent gait cycle (Subject 5)*. The seven trials were combined to produce mean angular momenta with error bars given by one standard deviation. L_x varies between -2.6 $kg \cdot m^2/s$ and 2.0 $kg \cdot m^2/s$, L_y between -3.0 $kg \cdot m^2/s$ and 5.4 $kg \cdot m^2/s$, and L_z between -1.1 $kg \cdot m^2/s$ and 1.2 $kg \cdot m^2/s$.

35

3.3.2 Principal Components

PCA was done on the link angular momenta as detailed in Section 3.2. Figures 3-6 through 3-10 show the percent variance in total angular momentum explained by the first five principal components. For each subject, PCA was done on the link angular momenta combined from all walking trials. The first PC explained most of the variance in angular momentum in each case.

Figure 3-6: *Percent variance in angular momentum explained by first five principal components (Subject 1).* The first PC of L_x explains 78.3% of the variance in L_x. The first PC of L_y explains 85.6% of the variance in L_y. The first PC of L_z explains 93.1% of the variance in L_z.

Figure 3-7: *Percent variance in angular momentum explained by first five principal components (Subject 2).* The first PC of L_x explains 74.6% of the variance in L_x. The first PC of L_y explains 85.7% of the variance in L_y. The first PC of L_z explains 91.4% of the variance in L_z.

Figure 3-8: *Percent variance in angular momentum explained by first five principal components (Subject 3).* The first PC of L_x explains 70.0% of the variance in L_x. The first PC of L_y explains 86.8% of the variance in L_y. The first PC of L_z explains 91.9% of the variance in L_z.
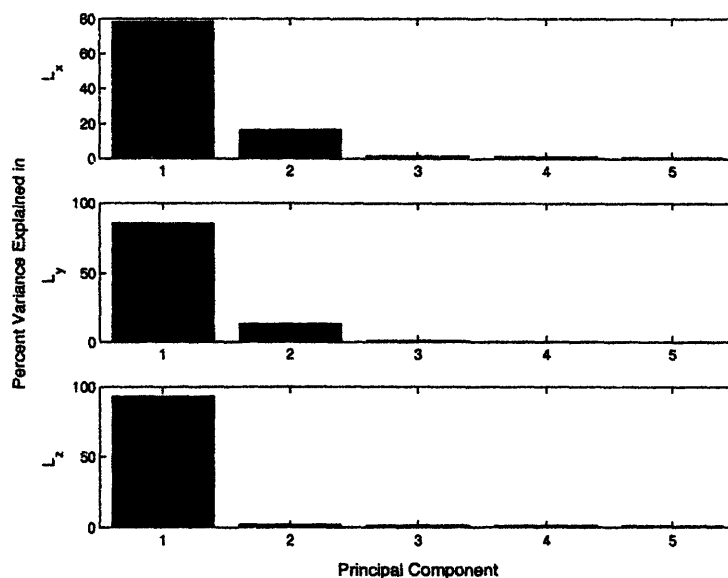
Figure 3-9: *Percent variance in angular momentum explained by first five principal components (Subject 4)*. The first PC of L_x explains 69.8% of the variance in L_x. The first PC of L_y explains 87.2% of the variance in L_y. The first PC of L_z explains 91.2% of the variance in L_z.
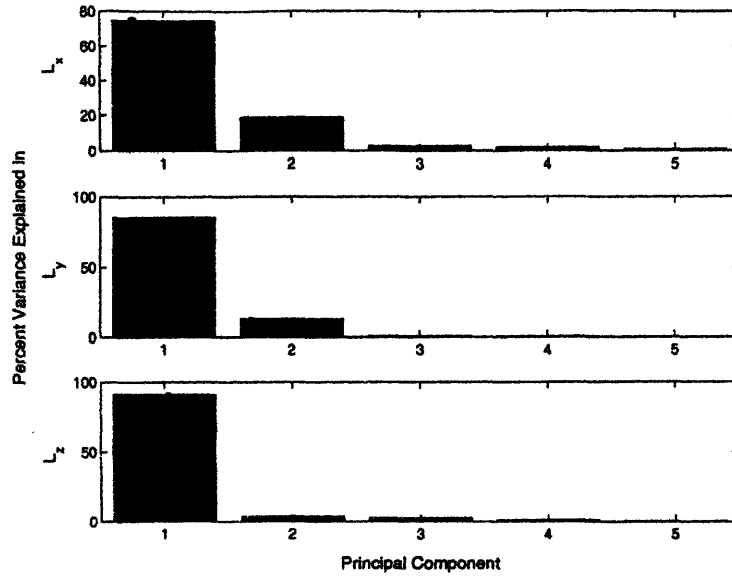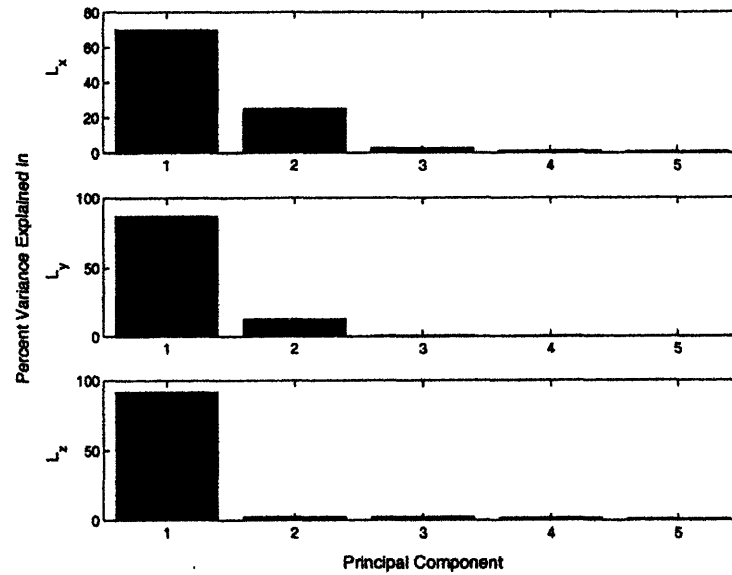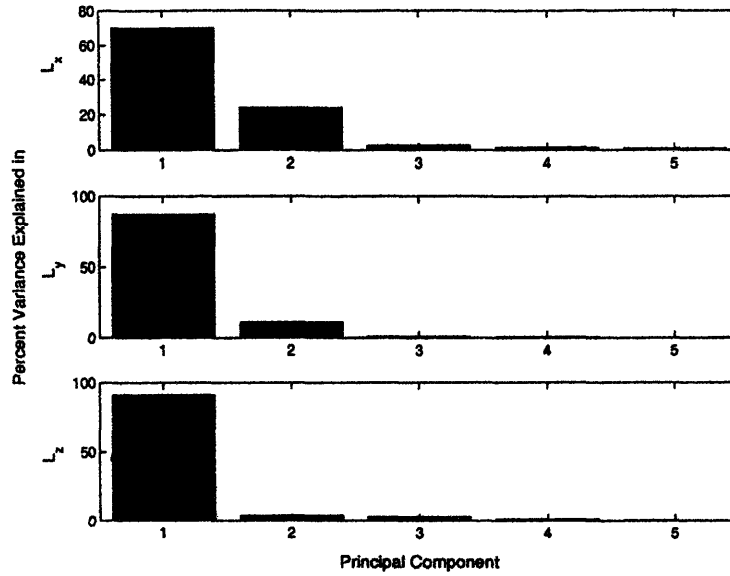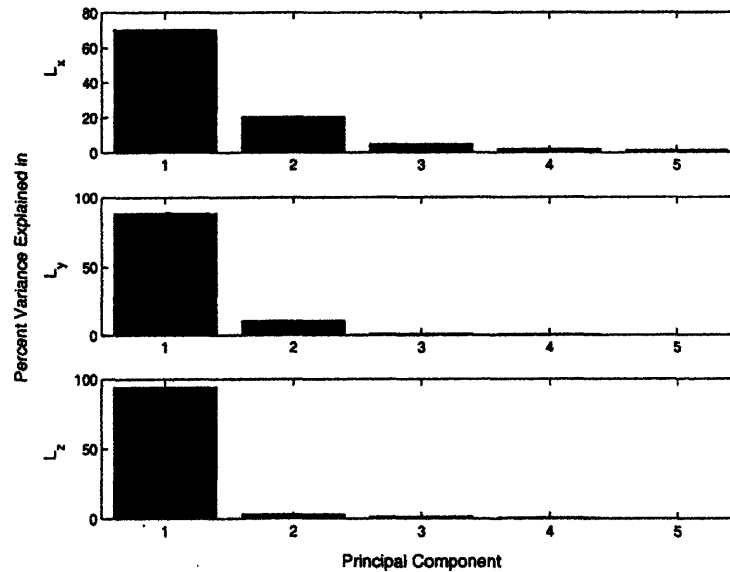

Figure 3-10: *Percent variance in angular momentum explained by first five principal components (Subject 5)*. The first PC of L_x explains 70.3% of the variance in L_x. The first PC of L_y explains 88.4% of the variance in L_y. The first PC of L_z explains 94.2% of the variance in L_z.

38

Subject	$\%s^2_{L_x}$	$\%s^2_{L_y}$	$\%s^2_{L_z}$
1	78.3	85.6	93.1
2	74.6	85.7	91.4
3	70.0	86.8	91.9
4	69.8	87.2	91.2
5	70.3	88.4	94.2
Mean	72.6 ± 3.8	86.7 ± 1.2	92.4 ± 1.3

Table 3.1: *Percent variance in angular momentum explained by first principal component.* The mean percent variance in L_x explained by the first PC of L_x ($\%s^2_{L_x}$) is lower than the mean $\%s^2_{L_y}$ and the mean $\%s^2_{L_z}$ and has a larger standard deviation. The standard deviation in the mean $\%s^2_{L_x}$ is comparable to that in the mean $\%s_{L_y}$, though the mean $\%s^2_{L_x}$ is larger.

A summary of percent variance in L_x, L_y, and L_z explained by the first PC of each and the mean and standard deviation for each quantity across the five subjects are displayed in Table 3.1. The mean percent variance in L_x, L_y, and L_z explained by its first PC was, respectively, $72.6\% \pm 3.8\%$, $86.7\% \pm 1.2\%$, and $92.4\% \pm 1.3\%$. The link-to-number correspondence in Figures 3-11 through 3-15 is given in Table 3.2.

Number	Link
1	left foot
2	right foot
3	left shank
4	right shank
5	left thigh
6	right thigh
7	left hand
8	right hand
9	left forearm
10	right forearm
11	left upper arm
12	right upper arm
13	trunk and head

Table 3.2: *Link-to-number correspondence.* Each link is assigned a number to ease reading of the x-axis in Figures 3-11 through 3-15.

The relative contribution of the body links listed in Table 3.2 to the first PC of angular momentum for each subject is shown by Figures 3-11 through 3-15. Some general trends appeared across subjects. The largest contributions to the first PC of L_x came from the feet, shanks, and trunk and head. The feet and shanks carried the most weight in the first PC of L_y. For the first PC of L_z, the shanks and thighs were the major contributors.

Figure 3-11: *Relative contribution of body links to first principal component (Subject 1)*. The largest contributions to the first PC of L_x come from the feet (Links 1 and 2), shanks (Links 3 and 4), and trunk and head (Link 13). The feet and shanks carry the most weight in the first PC of L_y. For the first PC of L_z, the shanks and thighs (Links 5 and 6) are the major contributors

Figure 3-12: *Relative contribution of body links to first principal component (Subject 2)*. The largest contributions to the first PC of L_x come from the feet (Links 1 and 2), shanks (Links 3 and 4), and trunk and head (Link 13). The feet and shanks carry the most weight in the first PC of L_y. For the first PC of L_z, the shanks and thighs (Links 5 and 6) are the major contributors
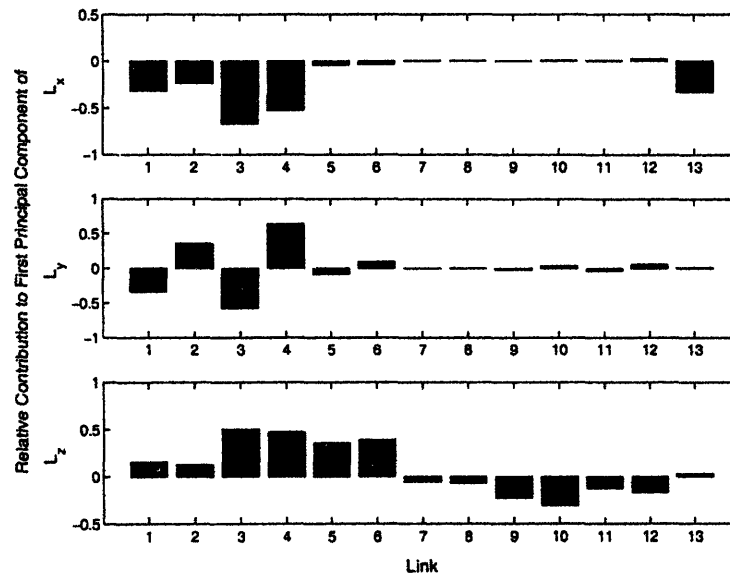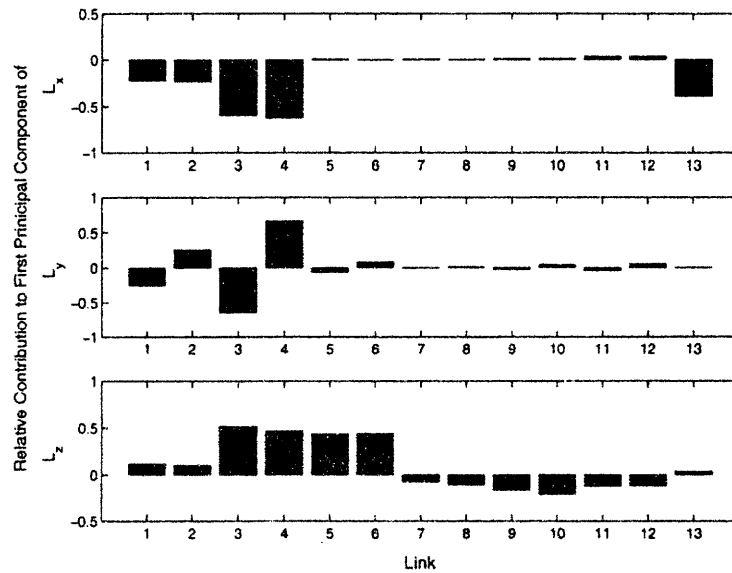

Figure 3-13: *Relative contribution of body links to first principal component (Subject 3)*. The largest contributions to the first PC of L_x come from the feet (Links 1 and 2), shanks (Links 3 and 4), and trunk and head (Link 13). The feet and shanks carry the most weight in the first PC of L_y. For the first PC of L_z, the shanks and thighs (Links 5 and 6) are the major contributors
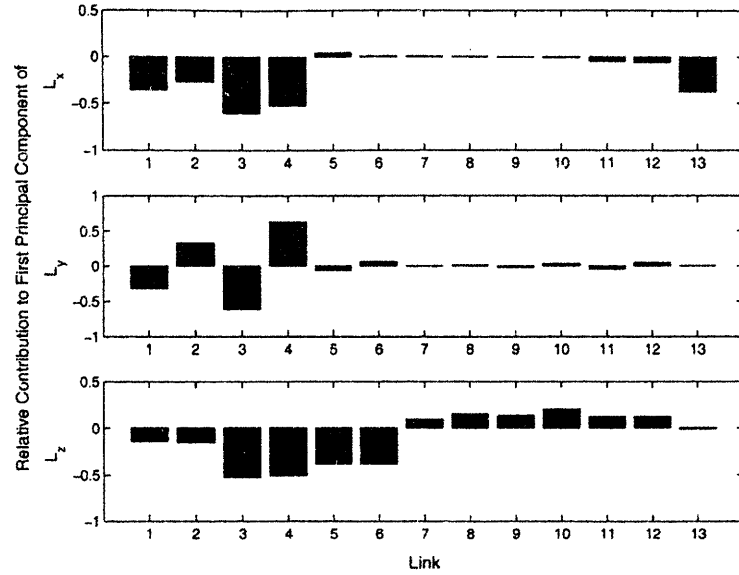
Figure 3-14: *Relative contribution of body links to first principal component (Subject 4)*. The largest contributions to the first PC of L_x come from the feet (Links 1 and 2), shanks (Links 3 and 4), and trunk and head (Link 13). The feet and shanks carry the most weight in the first PC of L_y. For the first PC of L_z, the shanks and thighs (Links 5 and 6) are the major contributors
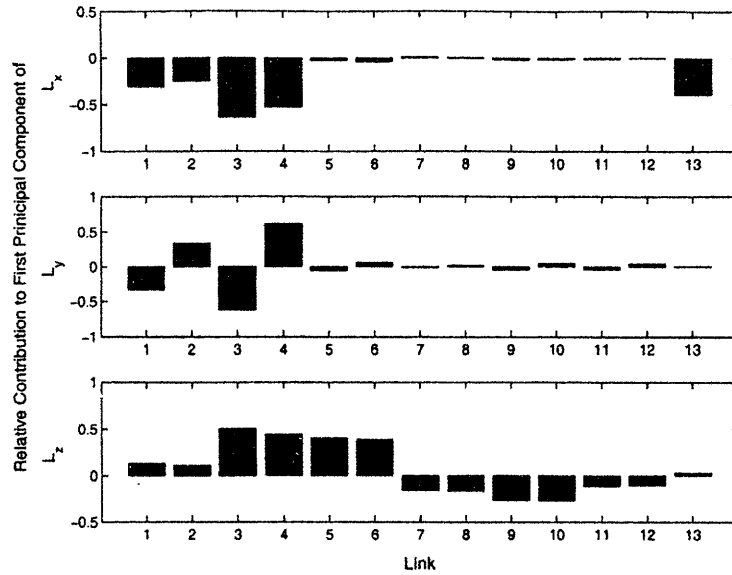

Figure 3-15: *Relative contribution of body links to first principal component (Subject 5)*. The largest contributions to the first PC of L_x come from the feet (Links 1 and 2), shanks (Links 3 and 4), upper arms (Links 11 and 12), and trunk and head (Link 13). The feet and shanks carry the most weight in the first PC of L_y. For the first PC of L_z, the shanks and thighs (Links 5 and 6) are the major contributors.
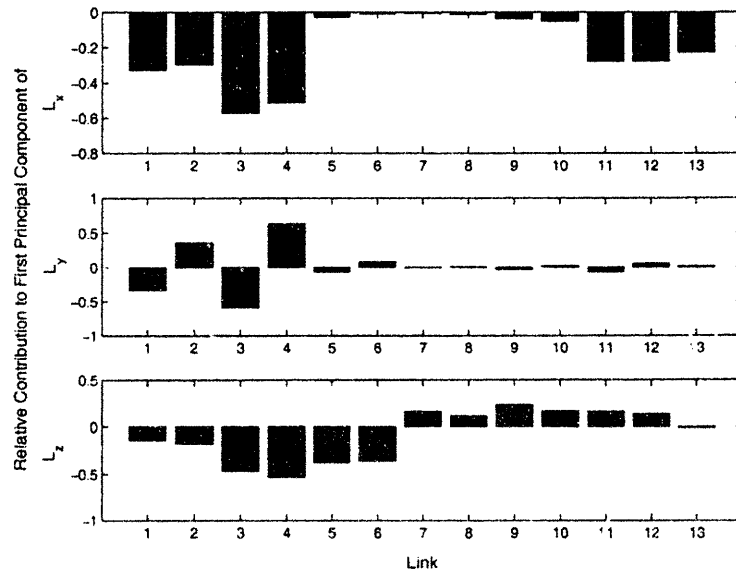
3.4 Discussion

The first principal component of L_x, L_y, and L_z accounted for, respectively, $72.6\% \pm 3.8\%$, $86.7\% \pm 1.2\%$, and $92.4\% \pm 1.3\%$ of the variance in those quantities (Table 3.1). This suggests that instead of describing the total angular momentum by considering the sum of thirteen individual links, we can use just one variable to explain a great deal of the total angular momentum: the first principal component. Insight into the partition of angular momentum, in other words how the body uses various links to regulate angular momentum, can be gained by examining the contribution of each link to the first principal component (Figures 3-11 through 3-15).

In the case of L_y, the major contributors to the first PC were the links of the lower body. The antisymmetry of the bars for left and right feet indicates that the angular momenta of these two links cancel each other during walking. The same reasoning applies to the pair of shanks and pair of thighs. L_y, which is the key angular momentum to regulate because it is the largest angular momentum link by link, showed almost perfect cancellation.

For L_z, the opposite signs of the bars for the lower and upper body links suggest that the angular momenta of the lower and upper body cancel each other in part. The cancellation was not as perfect as it was for L_y because the bars do not sum to zero. The body is less likely to become unstable from small values of angular momentum, and since L_z was much smaller than L_y link by link, complete cancellation was not as vital in the z direction.

The link contribution profile to the first PC of L_x indicates that there was no cancellation among the links, yet L_x was still small compared to L_y (Figures 3-1 through 3-5). This is possible if the body minimizes L_x of each link independently, and each link L_x points in roughly the same direction during walking. PCA would not be sensitive to this sort of control mechanism. This phenomenon could also account for the incomplete cancellation seen in L_z.

Chapter 4

Conclusion

4.1 Future Work

The next step is to expand the study to additional subjects and to determine how factors such as walking speed and body morphology affect angular momentum regulation. To investigate the effect of walking speed, the subject will walk slower or faster than his or her self-selected speed. The results of this experiment will be compared to the experiment at the self-selected speed. Weights will be attached to the subject's arm or leg during walking to examine the effect of body morphology on angular momentum. Comparing these trials to the ones without weights, we expect that the angular momenta of the body and links will look similar with and without the weights. We hypothesize that the body will compensate for the additional angular momentum introduced by the attached weights by rotating other links faster to generate angular momentum to cancel the increased link angular momentum. Alternatively, the body could move the link with the weights more slowly to reduce the angular momentum contribution from that link.

In addition, force and angular momentum calculations will be improved by examining the validity of certain assumptions made during the analysis. First, the center of mass of each link was assumed to adhere to the norm established from anthropological data. Error in the link CM would affect force and angular momentum calculations. Also, angular momentum associated with rotations of each link about its own z axis

(the line joining two joints) was assumed to be very small compared to the other two angular momenta as not much twisting of the links occurs during walking. This would affect calculation of link angular momenta and thus total angular momentum.

4.2 Concluding Remarks

To determine the extent to which the body regulates angular momentum, a force model was developed to predict the GRF in the x and y directions assuming perfect angular momentum conservation. These model forces closely matched experimental forces, suggesting that the body does indeed regulate angular momentum. The angular momenta of the links of the body were calculated to determine the partition of angular momentum. We found that L_y and L_z showed evident cancellation of link angular momenta whereas L_x did not. Link by link, L_y was much larger than L_x and L_z, which makes it more likely to cause stability problems. Therefore, L_y is the key angular momentum to regulate. In the course of this work, a computer human model and software programs (*ForceCalc* and *LCalc*) were developed to analyze data.

Bibliography

[1] J. Dapena. An analysis of angular momentum in the discus throw. In *Proc. 14th International Congress of Biomechanics*, 1993.

[2] J. Dapena and C. McDonald. A three-dimensional analysis of angular momentum in the hammer throw. *Medicine and Science in Sports and Exercise*, 21:206–220, 1989.

[3] R. Hinrichs. Upper extremity function in running: Angular momentum considerations. *International Journal of Sport Biomechanics*, 3:242–263, 1987.

[4] R. Hinrichs. Case studies of asymmetrical arm action in running. *International Journal of Sport Biomechanics*, 8:111–128, 1992.

[5] R. Hinrichs, P. Cavanagh, and K. Williams. Upper extremity contributions to angular momentum in running. In *Proc. 8th International Congress of Biomechanics*, 1983.

[6] J. Jackson. *A User's Guide to Principal Components*. John Wiley & Sons, Inc., New York, NY, 1991.

[7] M. P. Kadaba, H. K. Ramakrishnan, M. E. Wooten, J. Gainey, G. Gorton, and G. V. B. Cochran. Repeatability of kinematic, kinetic, and electromyographic data in normal adult gait. *Journal of Orthopaedic Research*, 7(6):849–860, 1989.

[8] S. Kajita, K. Yokoi, M. Saigo, and K. Tanie. Balancing a humanoid robot using backdrive concerned torque control and direct angular momentum feedback. In

Proc. IEEE International Conference on Robotics and Automation, pages 3376–3382, May 2001.

[9] M. LeBlanc and J. Dapena. Generation and transfer of angular momentum in the javelin throw. In *Proc. 20th Annual Meeting of the American Society of Biomechanics*, October 1996.

[10] P. Riley, D. Krebs, and R. Popat. Biomechanical analysis of failed sit-to-stand. *IEEE Transactions on Rehabilitation Engineering*, 5(4):353–359, December 1997.

[11] A. Sano and J. Furusho. Realization of natural dynamic walking using the angular momentum information. In *Proc. IEEE International Conference on Robotics and Automation*, pages 1476–1481, May 1990.

[12] G. Simoneau and D. Krebs. Whole-body angular momentum during gait: A preliminary study of non-fallers and frequent fallers. *Journal of Applied Biomechanics*, 16:1–13, 2000.

[13] D. Xu and T. Wang. Lower extremity contributions to altering direction during walking: Analysis of angular momentum. In *Proc. North American Congress on Biomechanics*, August 1998.